Development, Growth & Differentiation
The Japanese Society of Developmental Biologists
Develop. Growth Differ. (2017) doi: 10.1111/dgd.12366

Review Article

Determining the impact of cell mixing on signaling during development

Koichiro Uriu[1]* and Luis G. Morelli[2,3,4]

[1]*Graduate School of Natural Science and Technology, Kanazawa University, Kakuma-machi, Kanazawa 920-1192, Japan;* [2]*Instituto de Investigación en Biomedicina de Buenos Aires (IBioBA) – CONICET – Partner Institute of the Max Planck Society, Godoy Cruz 2390, C1425FQD, Buenos Aires, Argentina;* [3]*Department of Systemic Cell Biology, Max Planck Institute for Molecular Physiology, Otto-Hahn-Str. 11, 44227, Dortmund, Germany; and* [4]*Departamento de Física, FCEyN, UBA, Pabellon 1, Ciudad Universitaria, 1428 Buenos Aires, Argentina*

Cell movement and intercellular signaling occur simultaneously to organize morphogenesis during embryonic development. Cell movement can cause relative positional changes between neighboring cells. When intercellular signals are local such cell mixing may affect signaling, changing the flow of information in developing tissues. Little is known about the effect of cell mixing on intercellular signaling in collective cellular behaviors and methods to quantify its impact are lacking. Here we discuss how to determine the impact of cell mixing on cell signaling drawing an example from vertebrate embryogenesis: the segmentation clock, a collective rhythm of interacting genetic oscillators. We argue that comparing cell mixing and signaling timescales is key to determining the influence of mixing. A signaling timescale can be estimated by combining theoretical models with cell signaling perturbation experiments. A mixing timescale can be obtained by analysis of cell trajectories from live imaging. After comparing cell movement analyses in different experimental settings, we highlight challenges in quantifying cell mixing from embryonic timelapse experiments, especially a reference frame problem due to embryonic motions and shape changes. We propose statistical observables characterizing cell mixing that do not depend on the choice of reference frames. Finally, we consider situations in which both cell mixing and signaling involve multiple timescales, precluding a direct comparison between single characteristic timescales. In such situations, physical models based on observables of cell mixing and signaling can simulate the flow of information in tissues and reveal the impact of observed cell mixing on signaling.

Key words: cell movement, coupled oscillators, Delta-Notch signal, mean squared displacement, synchronization.

Introduction

Information flow by intercellular signaling organizes collective cellular behaviors both in tissues and cell aggregates. During embryonic development, signaling may occur simultaneously with cell movement. In some situations, cells use local biochemical signaling such as those mediated by membrane proteins or by slowly diffusing molecules. The resulting interaction range of such local biochemical signaling can be smaller than tissue size. In such cases, the movement of cells relative to their neighbors can cause rearrangements that change cells neighbors and affect the flow of information in the tissue. Most previous studies in development analyzed how signaling affects movement to generate collective cellular behaviors. In contrast, it is less understood how cell movement affects local intercellular signaling and changes information flow in developing tissues (Uriu *et al.* 2014).

To test whether cell mixing, which we define as the relative movement of cells, affects intercellular signaling, the comparison of movement and signaling timescales is an essential step. If the movement timescale is much slower than the signaling timescale, the effect of relative cell movement on information flow can be negligible. In contrast, if cells change their relative positions before signaling completes, movement might affect the signaling outcome, resulting in organized cellular behaviors that differ from those observed in a population of non-mobile cells.

*Author to whom all correspondence should be addressed.
Email: uriu@staff.kanazawa-u.ac.jp
Received 13 March 2017; revised 28 April 2017; accepted 29 April 2017.

In this article, we discuss how we can compare these two timescales to examine the influence of cell mixing on signaling, the difficulties and pitfalls that arise and strategies to overcome them. For this, we focus on the example of zebrafish somitogenesis where cell mixing and signaling occur simultaneously. This model system has the advantage that the effect of mixing on information flow has a clear readout in the synchronization dynamics of coupled genetic oscillators. Interplays between cell mixing and signaling in other developmental tissues are reviewed in Uriu *et al.* (2014). Here we first introduce zebrafish somitogenesis and the segmentation clock as a system of coupled genetic oscillators. Readers who are also interested in somitogenesis in other species can refer to Pourquie (2011), Kageyama *et al.* (2012), Saga (2012), Hubaud & Pourquie (2014). We next review theoretical work that shows how the ratio of timescales between mixing and signaling changes the collective behaviors of coupled oscillators. Then, we discuss quantification of cell movement using live imaging. We compare movement analysis in cell culture experiments with analysis in embryonic experiments to highlight a problem specific to embryonic tissues. We also mention how to define and quantify signaling timescales using both theory and experiment. Finally, we conclude that physical modeling of cell mixing and signaling would be a powerful tool to unravel the interplay between them.

Mobile genetic oscillators in zebrafish somitogenesis

Somites are repetitive embryonic structures that differentiate into various tissues such as vertebra, limb and muscles in later developmental stages of vertebrates. Each somite buds off from the unsegmented presomitic mesoderm (PSM). In vertebrates, somites form rhythmically, one by one from anterior to posterior (Fig. 1A). Somitogenesis period is species specific and in zebrafish it is roughly 30 min. Rhythmic gene expression can be observed in cells in the PSM and tailbud (Delaune *et al.* 2012; Soroldoni *et al.* 2014) and the period of rhythmic gene expression sets the timing when the next somite is formed. These cyclic genes include *her1*, *her7* and *deltaC* in zebrafish (Krol *et al.* 2011). The presence of delayed negative feedback of Her1 and Her7 proteins (Fig. 1B) (Lewis 2003; Schroter *et al.* 2012; Hanisch *et al.* 2013) leads to the hypothesis that the oscillation of gene expression is cell-autonomous. A recent experimental study shows that isolated PSM cells indeed exhibit noisy oscillations of gene expression (Webb *et al.* 2016).

The genetic oscillations need to be synchronized across the PSM to make correct segments. Given the

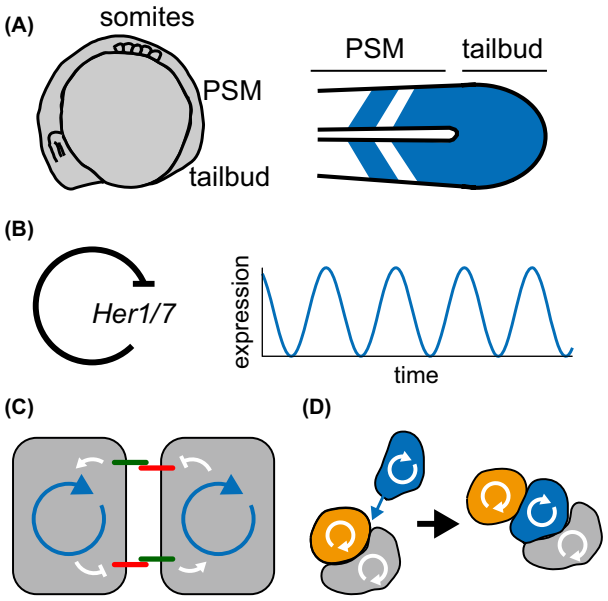

Fig. 1. Mobile genetic oscillators in the zebrafish segmentation clock. (A) Left: lateral outline of a zebrafish embryo. Right: dorsal view of gene expression pattern observed in the presomitic mesoderm (PSM) and tailbud. (B) Negative feedback loops by *her1* and *her7* in single cells produce oscillatory gene expression. (C) Neighboring cells interact with each other by Delta-Notch signaling. (D) Cells change relative positions due to movement. Local synchronization is perturbed by such cell mixing.

presence of noise in gene expression and cell divisions in the tissue that affect the phase of *her* genes oscillations (Horikawa *et al.* 2006; Delaune *et al.* 2012), cells in the PSM and tailbud must have a mechanism to maintain synchronization of their genetic oscillations. Cells in the PSM and tailbud express Delta and Notch proteins on their membrane (Wright *et al.* 2011) and interact with each other through Notch signaling (Fig. 1C) (Jiang *et al.* 2000; Horikawa *et al.* 2006; Riedel-Kruse *et al.* 2007; Ozbudak & Lewis 2008). Because Her proteins repress the transcription of *deltaC*, DeltaC protein levels also oscillate (Wright *et al.* 2011). Thus, cells can send information about their phase of oscillation to neighboring cells. Cells in the PSM and tailbud can therefore be considered as locally coupled oscillators. In the tailbud spatially uniform synchronization of genetic oscillators is observed (Soroldoni *et al.* 2014). In the PSM spatial kinematic phase waves are observed as a consequence of local synchronization of oscillators and a spatial gradient of oscillator's frequency (Fig. 1A) (Soroldoni *et al.* 2014; Shih *et al.* 2015). For more details on zebrafish somitogenesis, readers can refer to (Oates *et al.* 2012; Webb & Oates 2016; Yabe & Takada 2016).

These cells with the genetic oscillators move around within the posterior PSM and tailbud (Mara *et al.*

2007), and it is thought that cell movement influences axis extension (Lawton *et al.* 2013; Manning & Kimelman 2015). Cells form protrusions such as lamellipodia in the direction of movement (Manning & Kimelman 2015). Several signaling molecules that control cell movement in the PSM have been identified. Fgf signaling activates cell movement and forms gradient along the anterior-posterior axis of the PSM. Fgf level is higher at the posterior and it decreases toward the anterior (Sawada *et al.* 2001). Thus, it is thought that Fgf gradient is responsible for the spatial gradient of cell mobility along the anterior-posterior axis (Lawton *et al.* 2013). In addition, it has been known that Wnt signaling also forms a spatial gradient along anterior-posterior axis (Bajard *et al.* 2014) and affects cell movement in zebrafish (Lawton *et al.* 2013). Previous studies quantified single cell movement to examine its effect on axis elongation of embryos (Dray *et al.* 2013; Lawton *et al.* 2013; Steventon *et al.* 2016). Perturbation of cell movement resulted in shorter axis formation compared to wildtype.

In addition to the effects on axis extension, time lapse imaging indicated that cells change their relative positions in the posterior PSM and tailbud due to movement (Mara *et al.* 2007). As described above, Notch receptor and its ligands are transmembrane molecules and cells need to be touching each other for signals to take place. Hence, the fact that cells exchange neighbors over time becomes relevant to signaling events that mediate synchronization of oscillators. At first glance, cell mixing could be detrimental to synchronization (Fig. 1D). Neighboring cells with similar phase move apart, contact other cells with different phases and need to synchronize with these new neighbors. Thus, the observation of cell movement raises the question of how cell mixing in the posterior PSM and tailbud influences synchronization of genetic oscillators.

Theoretical studies on effect of cell mixing on synchronization of genetic oscillators

The question of how cell mixing affects synchronization of genetic oscillators in the zebrafish segmentation clock has been addressed in theory (Uriu *et al.* 2010). Theoretical studies show that the impact of mixing on synchronization depends on its timescale relative to the signaling timescale. In this section, we review these theoretical studies and related work on synchronization dynamics of mobile coupled oscillators.

To study the effect of cell mixing on synchronization of the zebrafish segmentation clock, Uriu *et al.* (2010, 2012) modeled cell mixing and coupled genetic oscillators. These theoretical studies suggest that cell mixing promotes synchronization of genetic oscillators in the segmentation clock. When cells do not exchange their neighbors, they tend to synchronize the phase of oscillation locally due to their limited interaction range, forming local synchronization domains. The dynamics are then confined to the boundaries between these locally synchronized domains and for this reason it takes a long time for non-mobile cells to attain global synchronization. In contrast, when cells exchange neighbors, they lose local synchronization as expected because each cell meets cells with a different phase value from the previous neighbors. However, frequent exchanges of neighbors destabilize persistent local phase patterns and lead to faster global synchronization. Thus, theory predicts that cell mixing can affect the outcome of local signaling.

The problem of synchronization of mobile entities is common to other areas of science and technology, for example communication networks (Wang *et al.* 2009) and robot swarming (Buscarino *et al.* 2006). This problem has been framed in the context of time varying networks (Skufca & Bollt 2004; Frasca *et al.* 2008; Fujiwara *et al.* 2011) and continuum descriptions (Peruani *et al.* 2010), and it poses an interesting paradigm for nonequilibrium statistical physics (Levis *et al.* 2017). Previous studies on agents on switching interaction networks have examined the characteristic time for attaining synchronization and stability of a synchronized state. A general question in the field is what is the rate of mobility of each agent, or alternatively the switching rate of an interaction network, required to enhance synchronization. Can even very slow cell mixing affect signaling?

As we discuss below, the extent of the impact of cell mixing on synchronization depends on how quickly cells exchange neighbors relative to how quickly they exchange signals. It is therefore important to define mixing and signaling characteristic timescales. The mixing timescale is how often cells exchange their neighbors, that is a waiting time to exchange neighbors. The waiting time might be difficult to measure in tissues, so one would need to estimate it by using other quantities. Signaling timescale is the time for internal gene expression (or cellular state) to be changed by intercellular interactions. For example, it is represented by the rate of change in phase due to intercellular interactions via Delta-Notch in the segmentation clock.

Interplay of timescales in coupled mobile oscillators

To examine how the system's behavior depends on the relation between the mixing and signaling timescales, Uriu *et al.* (2013) introduced a one-dimensional lattice of mobile coupled phase oscillators. An

advantage of using a lattice model is that it allows for simple definition of a mixing timescale as described below. There are other descriptions of cell movement such as cellular Potts model (Hester *et al.* 2011), using an off-lattice description of cells as self-propelled particles (Uriu & Morelli 2014), and continuum descriptions of coupled oscillators (Zhou & Kurths 2005; Ares *et al.* 2012; Jörg *et al.* 2015). More broadly, cell movement has been described and analyzed in the context of active matter theories (Vicsek *et al.* 1995; Ramaswamy 2010; Vicsek & Zafeiris 2012; Marchetti *et al.* 2013).

In the lattice model (Uriu *et al.* 2013), each oscillator exchanges its position with one of its two nearest neighbors in the lattice at random times at a rate λ (Fig. 2A). The waiting time for next exchange for a single oscillator is stochastic and its distribution obeys an exponential distribution. The average waiting time for an oscillator to exchange its location is $1/\lambda$. Then, the mixing timescale can be defined naturally as $T_m = 1/\lambda$. In other words, in this description, each oscillator performs a random walk on the one-dimensional lattice with diffusion coefficient λ.

Genetic oscillators in the one-dimensional lattice are described as a population of phase oscillators. Phase oscillator models have been used in the previous studies on biological rhythms including circadian clock (Liu *et al.* 1997; Yamaguchi *et al.* 2013) and the segmentation clock (Riedel-Kruse *et al.* 2007; Morelli *et al.* 2009). They are particularly useful when we consider the changes in phase of oscillation due to external stimuli such as light pulses and inputs from other oscillators. In general, the phase description of coupled genetic oscillators can be derived from a biochemical model by assigning the scalar value referred to as phase to the state space and applying linear approximation around a limit cycle (Kuramoto 1984).

For simplicity, Uriu *et al.* (2013) considers a population of identical phase oscillators with the natural frequency ω on the one-dimensional lattice. The phase dynamics of oscillators i ($i = 1, 2, \ldots, N$) is described as

$$\frac{d\theta_i(t)}{dt} = \omega + \frac{\kappa}{n_i}\sum \sin\left[\theta_j(t) - \theta_i(t)\right], \qquad (1)$$

where θ_i is the phase of oscillator i, κ is the coupling strength between two oscillators and n_i is the number of nearest neighbors in the one-dimensional lattice. The sinusoidal function represents coupling between two neighboring oscillators and reduces their phase differences. Oscillator i speeds up if it lags behind oscillator j, and slows down if it is ahead of oscillator j.

An advantage of using the phase oscillator model is that the signaling timescale can be defined straightforwardly. The coupling strength κ representing how fast the phase of oscillators θ_i changes due to local interactions (Fig. 2B) has units of inverse time. Thus, the signaling timescale can be defined as $T_s = 1/\kappa$ in the phase oscillator model. Biologically, the coupling strength is a coarse-grained parameter for the strength of Delta-Notch signaling. It would be an increasing function of Delta and Notch protein levels on cell membranes (Riedel-Kruse *et al.* 2007; Herrgen *et al.* 2010; Liao *et al.* 2016).

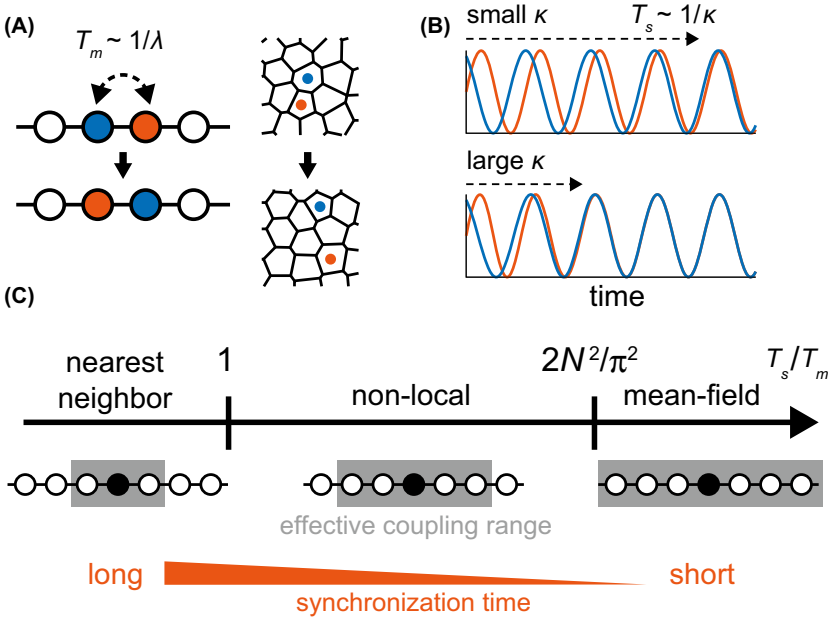

Fig. 2. Synchronization dynamics of mobile oscillators changes with the ratio of mixing to signaling timescales. (A) Left: neighbors in a one-dimensional lattice exchange their positions at a rate λ setting a mixing timescale T_m. Right: relative positional changes in an off-lattice model. Each polygon represents the shape of a cell. (B) The coupling strength κ sets the signaling timescale T_s. (C) Different regimes of synchronization dynamics induced by mixing.

Two timescales are present in the model: the mixing timescale T_m and the signaling timescale T_s. The behavior of population of phase oscillators depends on the ratio of mixing and signaling timescales T_s/T_m (Fig. 2C) (Uriu *et al.* 2013). In this simple model, there is an onset of non-local behavior at $T_s/T_m = 1$ where the mobility of oscillators begins to affect synchronization dynamics. When the ratio T_s/T_m is small ($T_s/T_m < 1$), the mobility of oscillators does not affect synchronization. Synchronization dynamics of these slow mobile oscillators is dominated by coupling and similar to that of non-mobile oscillators. They need longer time to reach global synchronization. When $T_s/T_m \approx 1$, the mobility of oscillators starts affecting synchronization. As the ratio increases ($T_s/T_m > 1$), the population of oscillators attains global synchronization more quickly. Note that the model suggests that the onset of non-local behavior does not depend on the system size N. This is because as soon as cells can exchange signals beyond their neighborhood by movement, their interaction range extends effectively (Fig. 2C) and the extended interaction range changes dynamics from that of oscillators with nearest neighbor coupling. Hence, the total cell number in a tissue is irrelevant when examining whether observed cell mixing can affect local signaling.

When T_s/T_m becomes sufficiently large, numerical simulations indicate that oscillators behave as if they were coupled with all the other oscillators in the lattice (Fig. 2C). Because mixing is so fast, each oscillator can interact with all the other oscillators before its phase changes significantly. The system with all-to-all coupling is referred to as a mean-field system in statistical physics. In this mean-field regime, the mobile oscillators attain global synchronization quickest. The onset of the mean-field behavior does depend on the system size or number of oscillators in the one-dimensional lattice as $T_s/T_m \sim N^2$ (Fig. 2C). For a larger system, oscillators need to move faster to behave as a mean-field coupling system. In actual biological systems, fast mixing may rather hamper signaling because cells cannot keep time to establish communication channels with their instantaneous neighbors. In such case, the timescale for building communication channels is also relevant (Uriu *et al.* 2012). Taken together, the relative timescales between mixing and signaling determines system's behavior in the simple one-dimensional lattice model.

Mixing in complex cell movement patterns

So far we considered a simple one-dimensional model in which cells' positions are constrained to a lattice. The above results also hold in an off-lattice model. Uriu & Morelli (2014) developed a two-dimensional off-lattice model where oscillators move around in a continuous domain (Fig. 2A). The model was motivated by the experimental observation that cells in the zebrafish tailbud and PSM move with positive velocity cross-correlations among them (Lawton *et al.* 2013). To describe such collective cell movement, Uriu & Morelli (2014) consider intrinsic cell movement, alignment of direction of movement and physical forces between neighboring cells. Using the model the authors examined the effect of collective cell movement on synchronization of coupled genetic oscillators. They showed that a short-range velocity correlation can enhance synchronization more than random cell movement, see also (Uriu 2016).

In the off-lattice model, defining the mixing timescale is not as simple as in the lattice model. If cell movement is a random walk, one can define the mixing timescale using the diffusion coefficient of cells as discussed for the one-dimensional lattice model. However, if cell movement is not a random walk but more complex, like including spatial velocity correlation, defining a single characteristic timescale of movement may be difficult. To quantify a mixing timescale in the off-lattice model, Uriu and Morelli defined the mean squared difference of displacement vectors (MSDD) (Uriu & Morelli 2014):

$$m(t) = \left\langle \left| \left\{ \mathbf{x}_j(t) - \mathbf{x}_j(t_0) \right\} - \left\{ \mathbf{x}_i(t) - \mathbf{x}_i(t_0) \right\} \right|^2 \right\rangle_{ij}, \quad (2)$$

where $\mathbf{x}_i$ and $\mathbf{x}_j$ are the positions of cells i and j in the two-dimensional space, t_0 is a reference time and $\langle \cdot \rangle_{ij}$ represents average over all possible pairs in the system. Essentially, the MSDD measures how fast the distance between two cells increases over time. Note that the MSDD is independent of a choice of a coordinate system in which cell positions are measured. This becomes important when quantifying cell mixing in embryonic tissues as we will see below. When the MSDD increases faster, two neighboring cells disperse quickly, indicating faster cell mixing. Uriu and Morelli used the first passage time t_e when the MSDD exceeds average cell diameter d_c for the first time in simulations $m(t_e) = d_c$. The first passage time is a rough representation of the waiting time for cells to exchange neighbors. In this way, the authors defined a mixing rate λ as $\lambda = 1/t_e$. Note that they introduced cell diameter d_c as a natural lengthscale to define mixing timescale.

Using the MSDD and first passage time, Uriu & Morelli (2014) observed that a short-range velocity correlation maximizes the degree of cell mixing,

consequently allowing oscillators to attain global synchronization quicker. Thus, movement patterns affect synchronization through changing the rate of cell mixing. In summary, the relation between mixing and signaling timescales is key in the off-lattice model as well.

Relevance to the segmentation clock in other species

We have discussed theory for zebrafish segmentation clock. Data for cell movement in the mouse PSM is still lacking but in the chick PSM cell movement was quantified previously (Delfini *et al.* 2005; Benazeraf *et al.* 2010; Oginuma *et al.* 2017). It was reported that chick cells perform a random walk in the PSM (Benazeraf *et al.* 2010; Oginuma *et al.* 2017). The speed of cell movement in the chick PSM (Delfini *et al.* 2005; Benazeraf *et al.* 2010; Oginuma *et al.* 2017) seems similar to that in the zebrafish PSM (Lawton *et al.* 2013), suggesting similar cell mixing timescale. How does cell mixing affect synchronization of genetic oscillators in other species?

The genetic regulatory network of the segmentation clock differs in complexity across species (Dequeant *et al.* 2006; Krol *et al.* 2011). In chick and mouse, in addition to Notch pathway, Fgf and Wnt pathways gene expression oscillates in the PSM whereas in zebrafish oscillatory expression is constrained to the Notch pathway (Krol *et al.* 2011). A remarkable difference among species is the timescale of somitogenesis (90 min in chick and 120 min in mouse). Because somitogenesis period in chick and mouse is longer than in zebrafish, signaling timescales might differ among species. The size of the PSM is also different among species and changes through development (Gomez *et al.* 2008). The chick and mouse have a longer PSM than zebrafish, indicating that tailbud size could also be larger in these species. These differences in tissue lengthscales could have a role on the synchronization at the tissue level because information has to propagate over longer distances. Therefore, larger tissues would benefit more from mixing to synchronize faster.

In light of these differences, cell mixing could be relevant to synchronization of genetic oscillations for other species as long as cell signaling is local. Because signaling timescale may differ among species, the impact of cell mixing on cell signaling may also differ even when cell mixing timescales are similar in different organisms.

Quantification of cell mixing timescale

In the previous section, we discussed how the effect of cell mixing on synchronization depends on the relative values of their corresponding timescales. Thus, quantification of these two timescales in the PSM and tailbud in zebrafish embryos is key to understanding the effect of cell mixing on the segmentation clock. Previously, observables for single cell movement such as cell velocity in these tissues have been measured (Lawton *et al.* 2013; Manning & Kimelman 2015). However, statistical observables for cell mixing, that are how cells move relative to their neighbors, are still lacking. Here we discuss how to quantify cell mixing in the embryonic tissues. To compute statistical observables for cell mixing, we first need to reliably track cells using live imaging.

Cell tracking and validation

Quantification of cell mixing in embryonic tissues starts with cell tracking, which is determining the position of cells within tissues over time. Tracking involves two separate steps: (i) identifying cells as distinct objects in the image at different times, which is segmentation, and (ii) linking the identity of a given cell across snapshots, referred to as linking. Various segmentation and linking algorithms for cells have been proposed (Sbalzarini & Koumoutsakos 2005; Li *et al.* 2007; Al-Kofahi *et al.* 2010; Qu *et al.* 2011; Amat *et al.* 2014; Stegmaier *et al.* 2014, 2016; Bhavna *et al.* 2016; Faure *et al.* 2016). Some algorithms perform segmentation and linking simultaneously using information of previous time frames (Qu *et al.* 2011; Amat *et al.* 2014). A general question would be which algorithm one should use to segment cells and link them between successive time frames. This would depend both on tissue properties such as cell density, cell size and cell velocity, and imaging conditions such as the kind of fluorophore that is used and whether it marks the cell nucleus or membrane, image size, spatial and temporal resolution, image contrast and signal-to-noise ratio determined by the quality of optics and camera. For cell movement analysis, labeling nuclei with Histone tag and tracking the center of each nucleus as a representative cell position may be enough. Alternatives are labeling cell membranes or whole cells, but segmentation and characterization of cells with such labelings may be harder than with nuclear labeling. A drawback of nuclear labeling though, is that nuclear motions within cells affect statistical observables of cell body motions (Liu *et al.* 2015). Simple threshold based methods might work sufficiently well to segment nuclei in tissues with low cell density (Keller *et al.* 2008). In contrast, in tissues with higher cell density such as the vertebrate PSM, more elaborate algorithms might be required to tell apart two (or more) touching nuclei. These algorithms use image intensity derivatives,

watershed, Gaussian mixture models and combinations.

Accurate nuclear segmentation and linking increase the accuracy of cell tracking. In general, there is a tradeoff between detection accuracy and computational time. Increasing accuracy typically requires longer computational time. Thus, one should determine to what extent accuracy of cell tracking will be needed before deciding which algorithm to use. Required accuracy would depend on the biological problem to be addressed (Bhavna *et al.* 2016). For example, if we analyze cell fate and lineage, we need very accurate cell tracking over a long time because individual cell identity is essential (Faure *et al.* 2016). In contrast, quantification of cell mixing may not need a very accurate algorithm because mixing can be characterized by quantities averaged over a population of hundreds of cells in local tissue domains, without the need to track for long times. Thus, assessment of accuracy required by the biological question addressed is fundamental for cell movement analysis.

To check the accuracy of an algorithm, we require ground truth datasets where we know the true positions and trajectories of cells. Some previous studies used manual segmentation and tracking of cells in embryonic tissues to obtain such ground truth (Li *et al.* 2007; Amat *et al.* 2014; Faure *et al.* 2016; Stegmaier *et al.* 2016). However, the human eye, good to detect objects and patterns, may also be subjected to systematic errors. In addition, obtaining a large number of datasets by manual annotations requires massive efforts. An alternative approach is to construct synthetic images that mimic an embryonic tissue by using a mathematical model (Bhavna *et al.* 2016). For instance, cell nuclei can be modeled as ellipsoids in a 3D space (Bhavna *et al.* 2016) while shapes of epithelial cells may be modeled as polygons in a 2D space. We can change parameters in synthetic images such as cell density, nuclear orientation, spatial and temporal resolution, background and signal-to-noise ratio, to calibrate image processing algorithms with images that have the same statistics as in the experimental conditions. In addition, defining appropriate measures for accuracy is key to validation and this depends on the biological question. For example, if the imaging time resolution is high enough compared to cell velocity, the degrees of over- and under-segmentation of nuclei or cells become most relevant as the main source of tracking error.

To complement this strategy, it would be good to obtain a large number of embryonic ground truth datasets. Dual labeling of cell nuclei by injection of mRNAs (Lawton *et al.* 2013) or transplantation of cells with a different nuclear labeling (Bhavna *et al.* 2016) can provide such datasets avoiding the need for manual tracking. In Bhavna *et al.* 2016, a small number of GFP-tagged cells from blastula stage zebrafish embryos was transplanted into stage matched mCherry-tagged host embryos. In the GFP channel, cell density is sparse because only transplanted cells are visible in the channel. Therefore, most nuclear segmentation algorithms can correctly segment these transplanted nuclei without problems. Thus, the segmentation result for the sparse channel can be considered as the ground truth dataset. The detection rate of the segmentation algorithm can be evaluated by comparing results for mCherry channel where all host cells are visible and density is high with the ground truth from GFP channel (Bhavna *et al.* 2016). This approach may be also applied for cell membrane makers to generate embryonic ground truth for cell membrane detection.

Typically, segmentation and tracking algorithms include several parameters that may need to be tuned for each specific embryonic image. Synthetic images and embryonic ground truth dataset provide a way to tune these parameters to the required level of accuracy.

Quantitative analysis of cell movement

From a dataset of cell trajectories we can compute statistical observables characterizing cell mixing in the PSM and tailbud. The characteristics of cell mixing depend on underlying cell movement patterns (Uriu & Morelli 2014). We first introduce quantification of movement in cell culture experiments to discuss basic properties of cell movement patterns. We show that some informative statistical observables can be derived from the analysis of cell displacement vectors in cell culture systems, revealing key movement features. Then, back to zebrafish somitogenesis, we point out pitfalls of relying on cell displacement vectors for analyzing embryonic experiments. We propose that relative displacement vectors between cells can be used to characterize cell mixing in embryonic tissues.

Movement analysis in cell culture experiments. Cell movement has been studied in cell culture experimental systems where experimental conditions may be strictly controlled. Because cells' behaviors can change with their density, the quantification methods may depend on the density of cells in the system. We first discuss analysis of single isolated cells. Then, we discuss cell movement analysis at higher cell density where a population of cells may exhibit collective movement.

Isolated single cell movement. Movement analysis of single isolated cells can reveal intrinsic properties of cell motility. The first step of quantification is to compute cell displacement vectors from cell trajectory data. To do this, we need to set a reference frame or coordinate system for analysis. The reference frame is the origin and axes of a spatial coordinate system from which the position of each cell is measured. Defining a reference frame in cell culture experiments is often straightforward because in most cases a lab reference frame can be introduced as a coordinate system fixed on the image. For example, the origin can be set at the top left corner of the image and axes defined along the image boundaries. Once a reference frame is set, the cell displacement vector $\Delta\mathbf{x}$ from the reference time t_0 can be computed, $\Delta\mathbf{x}(t) = \mathbf{x}(t + t_0) - \mathbf{x}(t_0)$. Using cell displacement vectors, various quantities can be obtained such as instantaneous cell velocity $\mathbf{v} = \Delta\mathbf{x}(t)/\Delta t$ and velocity auto-correlation for single cells. The mean squared displacement (MSD) is one of the most widely used quantities in cell movement analysis because its behavior hints about the type of movement that cells perform. The MSD is defined as

$$m_{\mathrm{d}}(t) = \left\langle |\mathbf{x}_i(t + t_0) - \mathbf{x}_i(t_0)|^2 \right\rangle_i, \qquad (3)$$

where $\langle\cdot\rangle_i$ denotes the average over a population of cells. Note that the MSD is based on the displacement vector $\Delta\mathbf{x}(t)$ of each cell. The MSD increases over time and its rate of increase is a measure of cell mobility. Very often the MSD is a power law function of time, $m_d(t) \propto t^{\alpha}$ and the value of the exponent α reveals the type of movement (Fig. 3A). When cell movement is a random walk, the MSD increases linearly over time ($\alpha \approx 1$) and its slope is an estimate of the diffusion coefficient of the cells (Gardiner 2009). The MSD may lose precision in estimating the diffusion coefficient when number of cells is limited and their trajectories are short. In such cases, the covariance between two successive displacement vectors can provide more accurate estimate of the diffusion coefficient (Vestergaard *et al.* 2015). In contrast, when a cell exhibits directed motion, for example in chemotaxis where cells are attracted by a chemical, the exponent α is close to two, $m_{\mathrm{d}}(t) \propto t^2$ (Fig. 3A). Such movement is called ballistic motion since it implies a movement with uniform velocity (Gardiner 2009).

In some cell types, the exponent of the MSD is in the range $1 < \alpha < 2$ (Fig. 3A). This type of anomalous diffusion is referred to as super-diffusion. Super-diffusion has been observed in Madin-Darby canine kidney (MDCK) cells (Dieterich *et al.* 2008) and Dictyostelium cells (Takagi *et al.* 2008). In these cells, it was also observed that the exponent of the MSD changes over time within the range $1 < \alpha < 2$, indicating the existence of different modes of cell movement. In the presence of anomalous diffusion, the distribution of cell positions at a given time t is

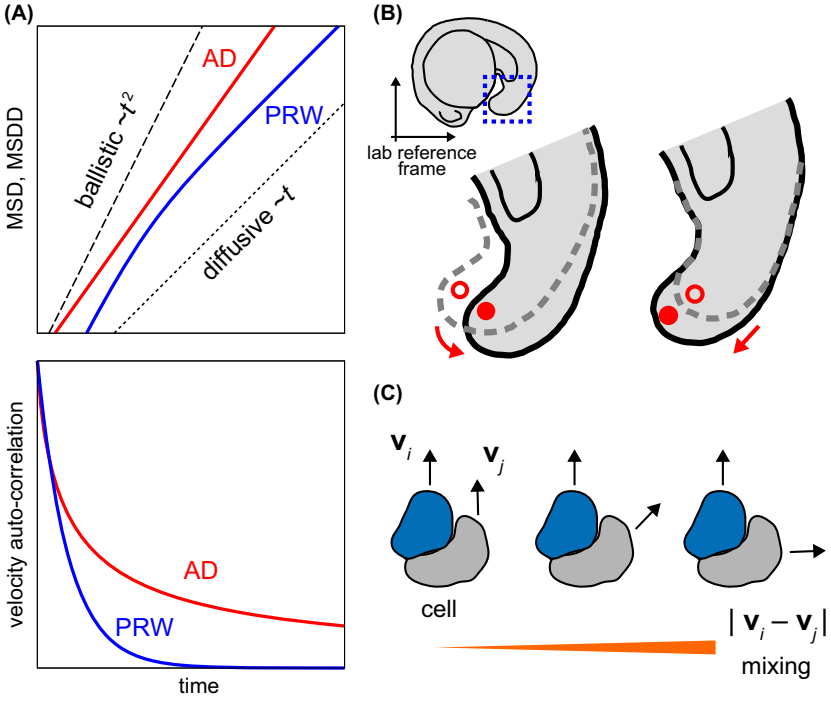

Fig. 3. Cell movement analysis in cell culture and embryonic experiments. (A) Top: Time evolution of mean squared displacement (MSD) and mean squared difference of displacement vectors (MSDD). Log scales in both vertical and horizontal axes. AD: anomalous diffusion. PRW: persistent random walk. Bottom: Time evolution of velocity auto-correlations. (B) Top: global tissue motions cause cell displacement in a lab reference frame. Left: an embryonic motion. Right: axis extension. Dashed and solid lines show embryonic outline before and after global motion. Open and solid dots show corresponding position of a given cell. (C) Difference of velocity vectors between neighboring cells.

non-Gaussian whereas it is Gaussian for normal diffusion (Dieterich *et al.* 2008; Takagi *et al.* 2008). Remarkably, a slower decay of velocity auto-correlation than exponential decay was observed in cells performing super-diffusion (Fig. 3A) (Upadhyaya *et al.* 2001; Dieterich *et al.* 2008). Hence, a long lasting memory of cell velocity would be an explanation for the emergence of the anomalous diffusive behaviors (Upadhyaya *et al.* 2001; Dieterich *et al.* 2008; Takagi *et al.* 2008).

Typically, a single cell moves in one direction for some characteristic time and then changes its direction of movement randomly. This characteristic time of the movement may be linked to dynamics of cell polarity molecules (Maiuri *et al.* 2015) and rearrangement of cytoskeletal networks. It is referred to as persistence time τ_p and signals a crossover in the MSD curve (Fig. 3A). At short time scale ($<\tau_p$), the MSD increases $\propto t^2$ because of cell's ballistic motion while at long time scale ($>\tau_p$) it increases $\propto t$ because of random changes in direction of motions. This type of movement is referred to as persistent random walk. The persistent time τ_p can be estimated by fitting the Furth formula for a persistent random walk model. The persistent random walk model was used to describe movement of various cells, including mouse fibroblasts cells (Gail & Boone 1970), mesenchymal cells (Liu *et al.* 2015), and endodermal Hydra cells (Rieu *et al.* 2000) on 2D substrates. Thus, the mode of cell movement appears different depending on the timescale of observation.

Importantly, even movement observables of a single isolated cell on 2D substrates contain several characteristic timescales. For instance, the exponent of the MSD changes over time, showing different migratory regimes (Dieterich *et al.* 2008; Takagi *et al.* 2008). The velocity auto-correlation for some cell types decays as a sum of two exponential functions (Selmeczi *et al.* 2005; Takagi *et al.* 2008; Li *et al.* 2011; Wu *et al.* 2014), indicating that at least two characteristic timescales are involved. In human WT fibrosarcoma HT1080 cells, such two characteristic timescales arise due to anisotropy of persistent time in primary and nonprimary directions of migration (Wu *et al.* 2014). In theory, fluctuations in the direction of movement may induce more than one crossover in the MSD at different timescales (Peruani & Morelli 2007). Multiple timescales may also reflect complex cellular processes like intracellular protein dynamics, formation of cellular protrusion and actual cell body motions. Thus, quantities based on cell displacement vectors characterize types of cell movement and can uncover the presence of different migratory modes within a single cell.

Collective cell movement. As cell density increases, cells are more likely to contact and interact with each other. A population of cells often changes behaviors depending on the density. For instance, diversity of movement behaviors of single fibroblast cells increases as a consequence of increasing cell density and intercellular interactions (Vedel *et al.* 2013). Epithelial cells undergo a transition of movement patterns that is reminiscent of a glass transition of a supercooled fluid with increasing cell density (Angelini *et al.* 2011) or with maturation of cell-cell and cell-surface interactions (Garcia *et al.* 2015). For some cell types such as fish keratocytes (Szabo *et al.* 2006), endothelial cells (Szabo *et al.* 2010) and mammalian epithelial cells like MDCK, MCF10A and HBEC (Haga *et al.* 2005; Tambe *et al.* 2011; Nnetu *et al.* 2012; Vedula *et al.* 2012; Garcia *et al.* 2015), it has been observed that long-range positive velocity cross-correlations arise when the cell density becomes high. Such correlated movement is referred to as collective cell movement. Active matter theory suggests that emergence of large scale, positive velocity correlations may result from local interactions (Vicsek *et al.* 1995; Chen *et al.* 2017), including physical contact forces between cells (Szabo *et al.* 2006) and cell shape dependent alignment (Peruani *et al.* 2006).

Collective cell movement has been observed in embryogenesis and wound healing (Friedl & Gilmour 2009; Rorth 2009) and extensively studied in cell culture experiments. A key step for quantifying migratory behaviors of a population of cells is to obtain a velocity field. The velocity field reveals spatial heterogeneity of speed (Angelini *et al.* 2011; Garcia *et al.* 2015) and characteristic movement patterns such as the existence of vortex motions (Vedula *et al.* 2012). The velocity field can be constructed using cell trajectories after tracking single cells. Another way to obtain a velocity field that does not require single cell tracking is to use particle image velocimetry (PIV). PIV obtains the direction of motion by computing cross-correlation of image intensity of local sub-domains between two successive time frames and determined the direction with the maximum cross-correlation (Angelini *et al.* 2011; Vedula *et al.* 2012; Garcia *et al.* 2015; Chen *et al.* 2017).

Various quantities that characterize migration patterns can be computed from the velocity field and cell trajectories. In addition to the single cell observables above, such as MSD and velocity auto-correlation, the velocity order parameter and velocity cross-correlation would be useful quantities to reveal to what extent a population of cells behaves collectively. The velocity order parameter is the modulus of the average velocity over a population of cells, which

quantifies the degree of alignment of velocities (Vicsek *et al.* 1995). Velocity cross-correlation between cells can be defined as

$$C(t) = \left\langle \frac{\mathbf{v}_i(t) \cdot \mathbf{v}_j(t)}{|\mathbf{v}_i(t)||\mathbf{v}_j(t)|} \right\rangle_{ij}, \quad (4)$$

where $\cdot$ indicates the inner product of vectors and $\langle \ldots \rangle_{ij}$ denotes the average over possible cell pairs. The cross-correlation C measures the angle between velocity vectors $\mathbf{v}_i$ and $\mathbf{v}_j$. If the angle is small, the two cells move in a same direction and C is close to 1. In contrast, if the angle is close to π, they move in opposite directions and C is close to -1. By using the cross-correlation, the lengthscale of collective cell movement can be quantified. Previous studies quantified the velocity correlation length for different cell types (Upadhyaya *et al.* 2001; Haga *et al.* 2005; Sepulveda *et al.* 2013; Garcia *et al.* 2015).

To reveal mechanisms that drive the observed collective cell movement, computing a correlation function between the direction of movement and presumptive factors would be useful. Previously, a positive correlation between the direction of polarization of collagen gel substrate and the direction of migration was observed for MDCK cells (Haga *et al.* 2005). Tambe *et al.* (2011) revealed correlation between the orientation of the local maximal principal stress in a cell sheet and the direction of the cell velocity vector for various cell types including MDCK cells. In HBEC populations, Garcia *et al.* (2015) detected a clear correlation between the strength of cell–cell, cell–surface interactions and velocity correlation length.

The MSD can also be used to quantify single cell motions when a population of cells undergoes collective movement. Typically, the exponent of the MSD tends to become larger than 1 for timescales where collective cell movement is observed (Haga *et al.* 2005; Nnetu *et al.* 2012). A population of MDCK cells moves collectively on a soft collagen gel surface and the exponents of their MSD curves are also larger than one, approximately 1.7 (Haga *et al.* 2005). Nearly ballistic motions of MCF-10A cells with an MSD exponent approximately 1.8 within a monolayer sheet ensure integrity of the migrating sheet of cells (Nnetu *et al.* 2012). Probably, longer persistence of direction of motions due to cell-cell interactions causes this super-diffusive behavior of the MSD. Again, in such cases the persistence time can be measured by temporal velocity auto-correlations of a single cell (Rieu *et al.* 2000; Upadhyaya *et al.* 2001; Sepulveda *et al.* 2013; Vedel *et al.* 2013).

We would like to emphasize that the statistical observables discussed so far rely on single cell displacement vectors measured in the lab reference frame of cell culture experiments. In these experimental systems, the only contribution to displacement vectors comes from cell movements, and therefore these statistical observables faithfully characterize movement properties.

Movement analysis in embryonic experiments. In contrast, one should be careful about using displacement vectors of single cells and derivative quantities to characterize cell movement in embryonic experimental systems. This is partly because embryos themselves can move under a microscope. The movement of an embryo causes a global tissue motion that can be decomposed in translation and rotation as in a rigid body (Feynman *et al.* 1963). Cell displacement vectors measured in the lab reference frame will include those contributions (Fig. 4). Besides these global motions, during development embryos can grow and change shape. For example, in zebrafish embryos, the tailbud progresses posteriorly due to axis extension and lifts from the yolk at around 15 somite stage (Fig. 3B). Such tissue deformation may also induce cell drifts (Morishita *et al.* 2015). Obviously, the MSD for single cells can be affected and its exponent tends to become larger than 1 due to persistence intrinsic to global tissue motions (Fig. 4). In addition, such global motions may give rise to strong cross-correlations of displacement vectors between cells, even though these cells move randomly within the tissue. Hence, measuring the degree of collective motions in embryonic tissues is often difficult and must be done carefully.

Therefore, if one wants to quantify single cells movement within embryos, setting an appropriate reference frame is key. If embryos move little under the microscope during imaging period and tissue deformation timescales are much slower than the process we are analyzing, we can set a lab reference frame and use movement observables as those discussed above for cell culture experimental systems. For example, interkinetic nuclear migration of neuroepithelial cells were analyzed in a slice culture system by computing the MSD of migrating nuclei at a lab reference frame (Norden *et al.* 2009). Another way to use the lab reference frame is to fix embryos by mounting them in agarose (Mara *et al.* 2007; Arboleda-Estudillo *et al.* 2010). Collective motions of mesoderm and endoderm progenitor cells during gastrulation of zebrafish embryos were characterized in this way using the MSD and velocity cross-correlations (Arboleda-Estudillo *et al.* 2010). Recently, an explant system of the zebrafish tailbud allowed cell movement in the tissue to be quantified

without being affected by global tissue motions (Manning & Kimelman 2015). The analysis revealed that wildtype cells in the tailbud explants moved in anterior direction with longer persistence than *tbx16:msgn1* morpholino knockdown cells (Manning & Kimelman 2015). While these strategies may circumvent the reference frame problem in some situations, they might introduce perturbations affecting the motion of cells in other contexts.

An alternative strategy to deal with tissue motions is to use an image registration algorithm that follows and subtracts embryonic movement on the microscope stage. Registration algorithms can correct for translations and rotations (Annila *et al.* 2013; Qu *et al.* 2015). After registration, a lab reference frame may be used. Although registration can also correct for tissue shape changes, if these occur on lengthscales comparable to cell displacements, image registration may introduce local deformations that alter the statistics of cell movement.

Thus, if global tissue motions are observed in the embryonic images, using a lab reference frame is problematic. In some cases, it may be possible to introduce an embryonic reference frame that can remove the contributions of global tissue motions (Fig. 4). For example, in the analysis of neural tube formation, the average position of a group of cells was used as a local reference frame for measuring movement of each cell in the group (Xiong *et al.* 2013). Previous studies that addressed axis extension of the vertebrate PSM set an embryonic reference frame using extracellular matrix (ECM) that drifts with surrounding cells (Benazeraf *et al.* 2010) or a tissue landmark in the anterior PSM (Lawton *et al.* 2013) to analyze cell movement. Such embryonic reference frames need to be correlated with global tissue motions (Fig. 4). The reference frame of the average position of a cell group removes contributions of global tissue motions but may introduce biases in estimation of diffusion coefficient of cells if the number of cells for averaging is small. ECM should not deform or move itself but rather be advected by tissue elongation and deformation. Motions of distant tissue domains need to be correlated strongly so that the anterior PSM functions as an embryonic reference frame for the region of interest.

If we are interested in relative cell movement or cell mixing, another strategy would be to use statistical observables that are based on cell pairs. Note that the observables for cell mixing and those for single cell movement are different, because cell mixing can be quantified by observing the motion of a cell in terms of other neighboring cells. By relying on an observable based on cell pairs, the movement components that are common to the pair such as global tissue motions due to embryonic movement, are cancelled out. Therefore, such observables do not depend on the choice of reference frame. For example, difference in velocity vectors between neighboring cells indicates local variations of cell velocity (Fig. 3C). Higher local variations of cell velocity suggest higher degree of cell mixing. Following this idea, one can compute the spatial derivative of velocity vectors. Because a velocity vector in a 3D space has three components $\mathbf{v} = (v_x, v_y, v_z)$ and there are three directions (x, y, z), this calculation provides a 3×3 matrix, the velocity gradient tensor, at each position in the tissue. Several characteristics can be derived from the velocity gradient tensor. For example, the eigenvalues of the matrix may represent the degree of local variations of velocity vectors. In addition, the determinant of the tensor reveals the rate of local tissue growth at each position. Such local measure of tissue growth will complement its global measures, like volumetric growth rate and axis extension rate of the PSM and somites (Steventon *et al.* 2016).

Another simple quantity for cell mixing that can be calculated from cell trajectories is the time evolution of the MSDD introduced before. By computing the difference of displacement vectors between two cells, the MSDD can also cancel out the contributions of global tissue motions (Fig. 4). As discussed before, the rate of MSDD increase represents the degree of cell mixing. In addition, similar to the MSD, the MSDD can reveal the type of cell movement by its exponent (Figs 3A and 4) (Uriu & Morelli 2014). A quantity similar to the MSDD was used previously to characterize motions of subcellular molecules when a cell itself moved under the microscopes (Marshall *et al.* 1997; Rafelski *et al.* 2011).

A drawback of using cell-pair-based quantities is that they do not reveal single cell velocities. One way to circumvent this issue and estimate properties of single cell movement in an embryonic tissue, such as cell velocity and velocity auto-correlation, is to use a physical model of cell movement. The physical model can be fitted to the statistical observables for cell mixing obtained from experiment, such as MSDD. Numerical simulations of the fitted model can allow for computing various movement observables that are difficult to measure in embryonic tissues. The results of the fitted model may be used to check whether an embryonic reference frame works properly by comparing movement observables of single cells from simulations with those from quantification at the embryonic reference frame. Thus, a physical model can complement the cell mixing dataset obtained from imaging data.

MSD and MSDD with global motions (*)

For simplicity, we consider an equation of motion for single cell moving in a one-dimensional space:

$$(1/\gamma)\dot{v}(t) = -v(t) + \sqrt{D}\xi(t), \quad \dot{x}(t) = v_G + v(t), \tag{1}$$

where v_G is contribution from global tissue motions and $\xi(t)$ is Gaussian white noise satisfying $\langle\xi(t)\rangle = 0$ and $\langle\xi(t_1)\xi(t_2)\rangle = \delta(t_1-t_2)$. We assume that v_G is constant. In this model, the MSD reads:

$$\left\langle \left\{x(t)-x(0)\right\}^2 \right\rangle = \left\langle \int_0^t \left(v_G + v(t_1)\right)dt_1 \int_0^t \left(v_G + v(t_2)\right)dt_2 \right\rangle. \tag{2}$$

Assuming an over-damped limit $1/\gamma << 1$ for simplicity, we obtain from Eq. (1) the relation:

$$v(t) = \sqrt{D}\xi(t). \tag{3}$$

Using Eq. (3), the MSD in Eq. (2) can be written as:

$$\left\langle \left\{x(t)-x(0)\right\}^2 \right\rangle = v_G^2 t^2 + Dt. \tag{4}$$

Thus, the MSD is affected by global motion at constant speed v_G. Diffusive motions can be detected with the MSD only if the experiment can resolve timescales below $D/{v_G}^2$.

Next, we evaluate the relation between the MSD and MSDD. The MSDD for two cells in a one-dimensional space is defined as:

$$m(t) = \left\langle \left[\left\{x(t)-x(0)\right\} - \left\{y(t)-y(0)\right\} \right]^2 \right\rangle. \tag{5}$$

Expanding Eq. (5), we obtain:

$$m(t) = \left\langle \left\{x(t)-x(0)\right\}^2 \right\rangle + \left\langle \left\{y(t)-y(0)\right\}^2 \right\rangle - 2\left\langle \left\{x(t)-x(0)\right\}\left\{y(t)-y(0)\right\} \right\rangle. \tag{6}$$

The first and second terms of Eq. (6) are the MSD for x and y, respectively. The last term of Eq. (6) is the covariance of displacement vectors. Considering over-damped dynamics for these two cells:

$$\dot{x}(t) = v_G + \sqrt{D_x}\xi_x(t), \; \dot{y}(t) = v_G + \sqrt{D_y}\xi_y(t), \tag{7}$$

the MSDs in Eq. (6) are:

$$\left\langle \left\{x(t)-x(0)\right\}^2 \right\rangle = v_G^2 t^2 + D_x t, \tag{8a}$$

$$\left\langle \left\{y(t)-y(0)\right\}^2 \right\rangle = v_G^2 t^2 + D_y t. \tag{8b}$$

If we assume that displacements $x(t)$–$x(0)$ and $y(t)$–$y(0)$ are independent, the covariance in Eq. (6) becomes:

$$\left\langle \left\{x(t)-x(0)\right\} \right\rangle \left\langle \left\{y(t)-y(0)\right\} \right\rangle = v_G^2 t^2. \tag{9}$$

Hence, the MSDD Eq. (6) reads:

$$m(t) = \left(D_x + D_y\right)t. \tag{10}$$

The assumption $\langle\xi_x(t_1)\xi_y(t_2)\rangle = \delta_{xy}(t_1-t_2)$ may brake at shorter timescales if the cells are very close together and additional terms may appear in Eqs. (9) and (10).

ECM reference frame

We consider the MSD in an ECM reference frame. Let x be the position of a cell of interest and y be the position of the ECM, such as fibronectin and fibrilin, near the cell. The position of the cell relative to the ECM is $x - y$. Then, the MSD of the cell relative to the ECM can be written as:

$$m_d(t) = \left\langle \left[\left\{x(t)-y(t)\right\} - \left\{x(0)-y(0)\right\} \right]^2 \right\rangle = \left\langle \left[\left\{x(t)-x(0)\right\} - \left\{y(t)-y(0)\right\} \right]^2 \right\rangle = m(t). \tag{11}$$

If we use same assumptions that used in the derivation of Eq. (10), the MSD is:

$$m_d(t) = \left(D_x + D_y\right)t, \tag{12}$$

where D_x and D_y are diffusion coefficients of the cell of interest and ECM, respectively. Thus, one can set the ECM as a local reference frame if the diffusion coefficient D_y is sufficiently smaller than D_x, that is $D_y/D_x << 1$. These results apply to other extracellular markers within the tissue that can serve as local references.

Average cell position reference frame

We consider a group of cells x_i (i = 1, 2,..., N) and measure cell positions from their average position $\bar{x}(t) = (1/N)\sum_{i=1}^{N} x_i(t)$. The MSD for cell i is:

$$m_d(t) = \left\langle \left[\left\{x_i(t)-\bar{x}(t)\right\} - \left\{x_i(0)-\bar{x}(0)\right\} \right]^2 \right\rangle. \tag{13}$$

By rearranging and expanding Eq. (13), we write the MSD as:

$$m_d(t) = \left\langle \left[\left\{x_i(t)-x_i(0)\right\} - \left\{\bar{x}(t)-\bar{x}(0)\right\} \right]^2 \right\rangle = \left\langle \left\{x_i(t)-x_i(0)\right\}^2 \right\rangle + \left\langle \left\{\bar{x}(t)-\bar{x}(0)\right\}^2 \right\rangle - 2\left\langle \left\{x_i(t)-x_i(0)\right\}\left\{\bar{x}(t)-\bar{x}(0)\right\} \right\rangle. \tag{14}$$

Assuming that fluctuations of different cells are uncorrelated as before:

$$\dot{x}_i(t) = v_G + \sqrt{D_i}\xi_i(t), \tag{15}$$

the MSD Eq. (14) becomes:

$$m_d(t) = D_i\left(1-1/N\right)t + \left(\bar{D} - D_i\right)t/N. \tag{16}$$

where $\bar{D} = \sum_{i=1}^{N} D_i/N$. Thus, if the number of cells N is small, the reference frame of average cell position biases the estimation of diffusion coefficient. To use the average cell position as a reference frame, $N >> 1$ and individual diffusion coefficients have to be narrowly distributed so $N >> \bar{D}/D_i$.

Anterior PSM reference frame

Assuming the motion of a tissue landmark, such as a reference point in the anterior PSM, is given by $X(t)$ with $\dot{X}(t) = V_G$, we obtain the MSD measured from this reference point after similar calculations:

$$\left\langle \left[\left\{x(t)-X(t)\right\} - \left\{x(0)-X(0)\right\} \right]^2 \right\rangle = \left(v_G - V_G\right)^2 t^2 + Dt. \tag{17}$$

Thus, if global motion of the anterior PSM is different from the region of interest due to tissue elongation and bending, then $v_G \neq V_G$ and this reference frame affects statistical observables of cell movement.

(*) Abbreviations are defined in the text.

Fig. 4. Statistical observables for cell mixing in embryonic experiments.

We have described the challenges posed by cell movement analysis in embryonic experiments, and outlined a number of strategies that have been proposed and employed. These strategies have their distinct advantages and drawbacks, and the choice of strategy should depend on the experimental system and question. We hope here we have provided some guidelines to facilitate this choice.

Quantification of signaling timescale

To quantify the impact of cell mixing on signaling we still need to determine the signaling timescale. In general, we expect this to be more difficult than determining the mixing timescale because it requires live imaging and time series analysis of the activity of a reporter gene related to the signaling event. For example, the timescale of Delta-Notch signaling may be determined by monitoring how fast activities of downstream genes change after an input signal. This challenging experiment was performed on Chinese hamster ovary cells plated on a Delta protein coated surface (Sprinzak *et al.* 2010). In this experimental system, Notch activity increases at the rate of several hours under the constant activation of Delta proteins (Sprinzak *et al.* 2010), which is much slower than the period of the segmentation clock. This observation suggests that the signaling timescale of Delta-Notch may strongly depend on cell types.

Theoretical models provide a way to indirectly determine the signaling timescale when combined with experiments. An advantage of a theoretical formulation of intercellular signaling is to rigorously specify what the signaling timescale represents within the formulation. One example is the coupling strength in a phase oscillator model (Kuramoto 1984). This coupling strength has not been directly measured in the zebrafish segmentation clock yet. Instead, it was estimated by fitting theory to experimental data (Fig. 5A) (Riedel-Kruse *et al.* 2007; Herrgen *et al.* 2010). Data for defective segments induced by inhibition of Delta-Notch signaling was used to estimate a coupling strength between cells in the context of a mean-field theory where every cell couples to every other cell (Kuramoto 1984; Pikovsky *et al.* 2001; Riedel-Kruse *et al.* 2007). In Delta-Notch mutants the first approximately five somites form normally, but defective segment boundaries appear after these normal somites. Treatment with a Delta-Notch signal inhibitor DAPT also causes segment defects after the formation of several normal somites (Fig. 5A). In the framework of the mean-field theory, these observations can be interpreted as arising from a decaying degree of phase synchronization, due to noise and a reduced coupling strength. When the degree of phase synchronization becomes lower than a critical value, only defective segments are formed (Riedel-Kruse *et al.* 2007; Liao *et al.* 2016). The coupling strength was estimated by fitting the mean-field coupling theory to the dependence of the anterior limit of defects (ALD) on DAPT treatment concentration, or antisense morpholino for *notch1a* mRNA concentration (Fig. 5A) (Riedel-Kruse *et al.* 2007). The estimated value of the coupling strength was about 0.07 min^{-1} (Riedel-Kruse *et al.* 2007). Another experiment used DAPT perturbation to determine the coupling strength (Herrgen *et al.* 2010). However, we defer its discussion to the next section where we consider multiple timescales in signaling. These two independent estimations of the coupling strength by Riedel-Kruse *et al.* (2007) and Herrgen *et al.* (2010) in the zebrafish segmentation clock gave a consistent value, $\kappa \sim 0.07\ \text{min}^{-1}$. Thus, combining theory with experimental perturbation of Delta-Notch signaling has allowed the coupling strength to be estimated in the context of a theory of coupled phase oscillators.

Still, direct measurement of the signaling timescale would be important because the estimated timescale may depend on theory, which is based on some assumptions. Direct quantification could be carried out by measuring how fast the phase difference between

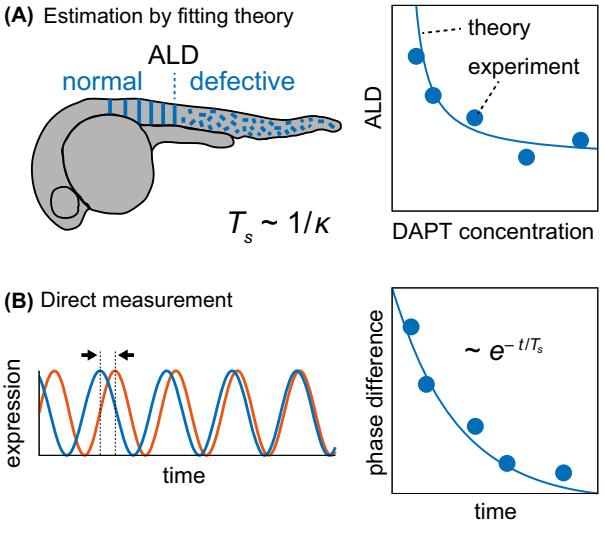

Fig. 5. Quantification of signaling timescale. (A) The signaling timescale can be determined from estimation of coupling strength κ, by fitting theory to experimental data of the anterior limit of defects (ALD) in zebrafish embryos. The solid blue lines indicate normal somite boundaries. ALD decreases with the increase of DAPT concentration. (B) Single cell observation of neighboring synchronizing oscillators allows the determination of the signaling timescale directly as a characteristic timescale of the phase difference decay.

two touching PSM cells decreases over time, with a live reporter of segmentation clock gene expression (Fig. 5B) (Aulehla *et al.* 2008; Delaune *et al.* 2012; Soroldoni *et al.* 2014; Shimojo *et al.* 2016). In cell culture experiments, a sparse cell population in a dish (Masamizu *et al.* 2006; Webb *et al.* 2016) would allow for such measurement. In embryos, the phases of oscillators become desynchronized with their neighbors after a cell division (Horikawa *et al.* 2006). It has been reported that the phases of divided cells tend to be delayed to those of surrounding undivided cells (Delaune *et al.* 2012). How fast these divided cells get synchronized back with surrounding cells in the tissue would reveal the coupling strength in the embryo.

More than one characteristic timescale: simulating the flow of information

If it is possible to determine a single timescale for cell mixing, such as a diffusion coefficient of cells, and one for signaling, such as the coupling strength, the effect of mixing on signaling could be elucidated based on theory as described above (Uriu *et al.* 2013). If the mixing timescale is faster than signaling timescale, mixing will affect signaling. However, it may happen that an experiment reveals more than one timescale associated either with mixing or signaling. In such case, a straightforward comparison is not possible and the theory has to be extended.

It may be difficult to determine a single characteristic timescale for cell mixing from cell movement statistical observables. For example, even isolated cells on a 2D substrate exhibit several timescales reflected in their MSD and velocity auto-correlation as described above (Selmeczi *et al.* 2005; Dieterich *et al.* 2008; Takagi *et al.* 2008; Li *et al.* 2011; Wu *et al.* 2014). In addition, cell movement may not be a simple random walk, as we have seen in examples of collective cell movement. Indeed, the exponent of the MSD for cells in the tailbud of zebrafish embryos was approximately 1.5 and, moreover, short-range velocity correlation was also reported (Lawton *et al.* 2013). Such complex cell movement with multiple timescales makes direct comparison between mixing and signaling difficult.

Multiple timescales can also occur in signaling, and this can impact dynamics and synchronization. For example, communication channels for signaling may need to build up after two cells come into contact due to mobility. As cells come in touch with each other their contact surface grows and receptor and ligand proteins on the cell membranes should associate to elicit new signals. This sets another timescale of recovering signaling after movement. A theoretical study showed that when this additional timescale is present there is an optimal mobility timescale that allows for fastest synchronization (Uriu *et al.* 2012). Communication delays introduce another timescale that can be relevant to signaling. Delta-Notch signaling involves time delays due to production and transport of Delta and Notch proteins (Morelli *et al.* 2009). In the framework of a delayed coupling theory (Morelli *et al.* 2009; Herrgen *et al.* 2010; Ares *et al.* 2012), the somitogenesis period is interpreted as a result of the collective period of cells. Phase oscillator models predict that the collective period is a function of the coupling strength κ given that Delta-Notch signal involves time delays. Remarkably, the somitogenesis period in living embryos changes depending on applied DAPT levels as predicted by the phase oscillator theory (Herrgen *et al.* 2010). Using this framework the coupling strength was also estimated, together with the coupling delay, from the change in somitogenesis period induced by DAPT treatment (Herrgen *et al.* 2010).

How can the impact of mixing on signaling be determined in such situations? Physical modeling of cell mixing and intercellular signaling could address this problem (Fig. 6). As we mentioned above, a model for cell movement can be fitted to the data of cell mixing obtained from live imaging. The fitted model allows us to simulate signaling dynamics in the presence of reproduced cell mixing. For the zebrafish segmentation clock, a coupled phase oscillator model can be combined with a fitted model for cell mixing in the PSM and tailbud. Such a combined model would simulate synchronization dynamics of the oscillators with

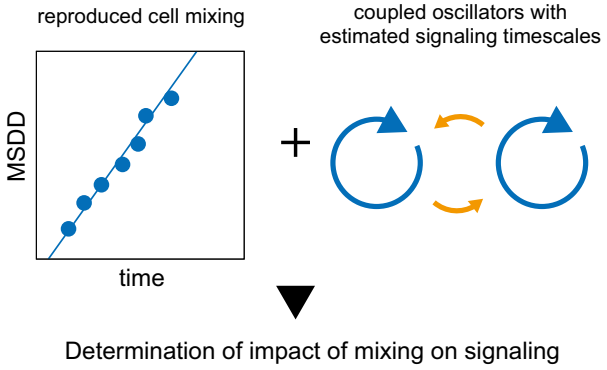

Fig. 6. Physical models quantifying the impact of cell mixing on cell signaling. Physical models can be developed that describe cell mixing and signaling, which can both display more than one characteristic timescale. Cell mixing in an embryonic tissue can be reproduced after fitting such a model to MSDD embryonic data. Together with signaling timescales determined by other experiments as shown in Figure 5, such a model would allow simulation of the flow of information in the tissue to determine the impact of mixing on signaling.

signaling events that may involve multiple timescales in reproduced cell mixing conditions. Using simulations would allow locating the system's behavior on a timescales map like the one established for the one-dimensional lattice model (Fig. 2C). The combined model could further predict how synchronization dynamics changes when the rate of cell mixing is reduced from its value as observed in wild type embryos. Such prediction could then be tested experimentally with a perturbation of cell mobility by drugs and quantification of synchronization level by the live reporter of the genetic oscillator. Thus, modeling may be essential when the determination of a single timescale characterizing mixing and signaling is not possible.

Conclusion

In this review article, we have argued that quantification of cell mixing and signaling timescales is essential to understand their interplay. Although advances in live imaging allows cell movement to be analyzed in embryonic experiments, careful setting of a reference frame is required to obtain statistical observables characterizing cell movement. Given that in embryos there are global cell motions like whole embryo movements and tissue shape changes, we argued that using movement observables that do not depend on a choice of a reference frame is paramount. Quantification of signaling timescale poses different challenges, but it can be carried out combining theory with the measurement of macroscopic observables. Physical modeling reveals the impact of cell mixing on signaling and provides experimentally testable predictions. Since cell movement and signaling are ubiquitous during morphogenesis, the approach proposed in this paper could be useful more broadly to understand the physical processes undergoing during embryonic development.

Acknowledgments

We thank Andrew Oates for helpful comments on the manuscript. This work was supported by JSPS KAKENHI Grant Number 26840085 to KU. LGM acknowledges support from ANPCyT grants PICT 2012 1952, PICT 2013 1301 and FOCEM-Mercosur (COF 03/11).

References

Al-Kofahi, Y., Lassoued, W., Lee, W. & Roysam, B. 2010. Improved automatic detection and segmentation of cell nuclei in histopathology images. *IEEE Trans. Biomed. Eng.* **57**, 841–852.

Amat, F., Lemon, W., Mossing, D. P., McDole, K., Wan, Y., Branson, K., Myers, E. W. & Keller, P. J. 2014. Fast, accurate reconstruction of cell lineages from large-scale fluorescence microscopy data. *Nat. Methods* **11**, 951–958.

Angelini, T. E., Hannezo, E., Trepat, X., Marquez, M., Fredberg, J. J. & Weitz, D. A. 2011. Glass-like dynamics of collective cell migration. *Proc. Natl Acad. Sci. USA* **108**, 4714–4719.

Annila, T., Lihavainen, E., Marques, I. J., Williams, D. R., Yli-Harja, O. & Ribeiro, A. 2013. ZebIAT, an image analysis tool for registering zebrafish embryos and quantifying cancer metastasis. *BMC Bioinformatics* **14**(Suppl 10), S5.

Arboleda-Estudillo, Y., Krieg, M., Stuhmer, J., Licata, N. A., Muller, D. J. & Heisenberg, C. P. 2010. Movement directionality in collective migration of germ layer progenitors. *Curr. Biol.* **20**, 161–169.

Ares, S., Morelli, L. G., Jorg, D. J., Oates, A. C. & Julicher, F. 2012. Collective modes of coupled phase oscillators with delayed coupling. *Phys. Rev. Lett.* **108**, 204101.

Aulehla, A., Wiegraebe, W., Baubet, V., Wahl, M. B., Deng, C., Taketo, M., Lewandoski, M. & Pourquie, O. 2008. A beta-catenin gradient links the clock and wavefront systems in mouse embryo segmentation. *Nat. Cell Biol.* **10**, 186–193.

Bajard, L., Morelli, L. G., Ares, S., Pecreaux, J., Julicher, F. & Oates, A. C. 2014. Wnt-regulated dynamics of positional information in zebrafish somitogenesis. *Development* **141**, 1381–1391.

Benazeraf, B., Francois, P., Baker, R. E., Denans, N., Little, C. D. & Pourquie, O. 2010. A random cell motility gradient downstream of FGF controls elongation of an amniote embryo. *Nature* **466**, 248–252.

Bhavna, R., Uriu, K., Valentin, G., Tinevez, J. Y. & Oates, A. C. 2016. Object segmentation and ground truth in 3D embryonic imaging. *PLoS One* **11**, e0150853.

Buscarino, A., Fortuna, L., Frasca, M. & Rizzo, A. 2006. Dynamical network interactions in distributed control of robots. *Chaos* **16**, 015116.

Chen, C., Liu, S., Shi, X. Q., Chate, H. & Wu, Y. 2017. Weak synchronization and large-scale collective oscillation in dense bacterial suspensions. *Nature* **542**, 210–214.

Delaune, E. A., Francois, P., Shih, N. P. & Amacher, S. L. 2012. Single-cell-resolution imaging of the impact of Notch signaling and mitosis on segmentation clock dynamics. *Dev. Cell* **23**, 995–1005.

Delfini, M. C., Dubrulle, J., Malapert, P., Chal, J. & Pourquie, O. 2005. Control of the segmentation process by graded MAPK/ERK activation in the chick embryo. *Proc. Natl Acad. Sci. USA* **102**, 11343–11348.

Dequeant, M. L., Glynn, E., Gaudenz, K., Wahl, M., Chen, J., Mushegian, A. & Pourquie, O. 2006. A complex oscillating network of signaling genes underlies the mouse segmentation clock. *Science* **314**, 1595–1598.

Dieterich, P., Klages, R., Preuss, R. & Schwab, A. 2008. Anomalous dynamics of cell migration. *Proc. Natl Acad. Sci. USA* **105**, 459–463.

Dray, N., Lawton, A., Nandi, A., Julich, D., Emonet, T. & Holley, S. A. 2013. Cell-fibronectin interactions propel vertebrate trunk elongation via tissue mechanics. *Curr. Biol.* **23**, 1335–1341.

Faure, E., Savy, T., Rizzi, B., Melani, C., Stasova, O., Fabreges, D., Spir, R., Hammons, M., Cunderlik, R., Recher, G., Lombardot, B., Duloquin, L., Colin, I., Kollar, J., Desnoulez, S., Affaticati, P., Maury, B., Boyreau, A., Nief, J. Y., Calvat, P., Vernier, P., Frain, M., Lutfalla, G., Kergosien, Y., Suret, P., Remesikova, M., Doursat, R., Sarti, A., Mikula, K., Peyrieras, N. & Bourgine, P. 2016. A workflow to process 3D+time

microscopy images of developing organisms and reconstruct their cell lineage. *Nat. Commun.* **7**, 8674.
Feynman, R. P., Leighton, R. B. & Sands, M. 1963. *The Feynman Lectures on Physics*, Vol. **1**. Addison-Wesley, Massachussetts.
Frasca, M., Buscarino, A., Rizzo, A., Fortuna, L. & Boccaletti, S. 2008. Synchronization of moving chaotic agents. *Phys. Rev. Lett.* **100**, 044102.
Friedl, P. & Gilmour, D. 2009. Collective cell migration in morphogenesis, regeneration and cancer. *Nat. Rev. Mol. Cell Biol.* **10**, 445–457.
Fujiwara, N., Kurths, J. & Diaz-Guilera, A. 2011. Synchronization in networks of mobile oscillators. *Phys. Rev. E Stat. Nonlin. Soft Matter Phys.* **83**, 025101.
Gail, M. H. & Boone, C. W. 1970. The locomotion of mouse fibroblasts in tissue culture. *Biophys. J.* **10**, 980–993.
Garcia, S., Hannezo, E., Elgeti, J., Joanny, J. F., Silberzan, P. & Gov, N. S. 2015. Physics of active jamming during collective cellular motion in a monolayer. *Proc. Natl Acad. Sci. USA* **112**, 15314–15319.
Gardiner, C. 2009. *Stochastic Methods*, 4th edn. Springer-Verlag, Berlin.
Gomez, C., Ozbudak, E. M., Wunderlich, J., Baumann, D., Lewis, J. & Pourquie, O. 2008. Control of segment number in vertebrate embryos. *Nature* **454**, 335–339.
Haga, H., Irahara, C., Kobayashi, R., Nakagaki, T. & Kawabata, K. 2005. Collective movement of epithelial cells on a collagen gel substrate. *Biophys. J.* **88**, 2250–2256.
Hanisch, A., Holder, M. V., Choorapoikayil, S., Gajewski, M., Ozbudak, E. M. & Lewis, J. 2013. The elongation rate of RNA polymerase II in zebrafish and its significance in the somite segmentation clock. *Development* **140**, 444–453.
Herrgen, L., Ares, S., Morelli, L. G., Schroter, C., Julicher, F. & Oates, A. C. 2010. Intercellular coupling regulates the period of the segmentation clock. *Curr. Biol.* **20**, 1244–1253.
Hester, S. D., Belmonte, J. M., Gens, J. S., Clendenon, S. G. & Glazier, J. A. 2011. A multi-cell, multi-scale model of vertebrate segmentation and somite formation. *PLoS Comput. Biol.* **7**, e1002155.
Horikawa, K., Ishimatsu, K., Yoshimoto, E., Kondo, S. & Takeda, H. 2006. Noise-resistant and synchronized oscillation of the segmentation clock. *Nature* **441**, 719–723.
Hubaud, A. & Pourquie, O. 2014. Signalling dynamics in vertebrate segmentation. *Nat. Rev. Mol. Cell Biol.* **15**, 709–721.
Jiang, Y. J., Aerne, B. L., Smithers, L., Haddon, C., Ish-Horowicz, D. & Lewis, J. 2000. Notch signalling and the synchronization of the somite segmentation clock. *Nature* **408**, 475–479.
Jörg, D. J., Morelli, L. G., Soroldoni, D., Oates, A. C. & Jülicher, F. 2015. Continuum theory of gene expression waves during vertebrate segmentation. *New J. Phys.* **17**, 093042.
Kageyama, R., Niwa, Y., Isomura, A., Gonzalez, A. & Harima, Y. 2012. Oscillatory gene expression and somitogenesis. *Wiley Interdiscip. Rev. Dev. Biol.* **1**, 629–641.
Keller, P. J., Schmidt, A. D., Wittbrodt, J. & Stelzer, E. H. 2008. Reconstruction of zebrafish early embryonic development by scanned light sheet microscopy. *Science* **322**, 1065–1069.
Krol, A. J., Roellig, D., Dequeant, M. L., Tassy, O., Glynn, E., Hattem, G., Mushegian, A., Oates, A. C. & Pourquie, O. 2011. Evolutionary plasticity of segmentation clock networks. *Development* **138**, 2783–2792.
Kuramoto, Y. 1984. *Chemical Oscillations, Waves, and Turbulence*. Springer-Verlag, Berlin.
Lawton, A. K., Nandi, A., Stulberg, M. J., Dray, N., Sneddon, M. W., Pontius, W., Emonet, T. & Holley, S. A. 2013. Regulated tissue fluidity steers zebrafish body elongation. *Development* **140**, 573–582.
Levis, D., Pagonabarraga, I. & Díaz-Guilera, A. 2017. Synchronization in dynamical networks of locally coupled self-propelled oscillators. *Phys. Rev. X* **7**, 011028.
Lewis, J. 2003. Autoinhibition with transcriptional delay: a simple mechanism for the zebrafish somitogenesis oscillator. *Curr. Biol.* **13**, 1398–1408.
Li, G., Liu, T., Nie, J., Guo, L., Malicki, J., Mara, A., Holley, S. A., Xia, W. & Wong, S. T. 2007. Detection of blob objects in microscopic zebrafish images based on gradient vector diffusion. *Cytometry A* **71**, 835–845.
Li, L., Cox, E. C. & Flyvbjerg, H. 2011. 'Dicty dynamics': Dictyostelium motility as persistent random motion. *Phys. Biol.* **8**, 046006.
Liao, B. K., Jorg, D. J. & Oates, A. C. 2016. Faster embryonic segmentation through elevated Delta-Notch signalling. *Nat. Commun.* **7**, 11861.
Liu, C., Weaver, D. R., Strogatz, S. H. & Reppert, S. M. 1997. Cellular construction of a circadian clock: period determination in the suprachiasmatic nuclei. *Cell* **91**, 855–860.
Liu, Y. J., Le Berre, M., Lautenschlaeger, F., Maiuri, P., Callan-Jones, A., Heuze, M., Takaki, T., Voituriez, R. & Piel, M. 2015. Confinement and low adhesion induce fast amoeboid migration of slow mesenchymal cells. *Cell* **160**, 659–672.
Maiuri, P., Rupprecht, J. F., Wieser, S., Ruprecht, V., Benichou, O., Carpi, N., Coppey, M., De Beco, S., Gov, N., Heisenberg, C. P., Lage Crespo, C., Lautenschlaeger, F., Le Berre, M., Lennon-Dumenil, A. M., Raab, M., Thiam, H. R., Piel, M., Sixt, M. & Voituriez, R. 2015. Actin flows mediate a universal coupling between cell speed and cell persistence. *Cell* **161**, 374–386.
Manning, A. J. & Kimelman, D. 2015. Tbx16 and Msgn1 are required to establish directional cell migration of zebrafish mesodermal progenitors. *Dev. Biol.* **406**, 172–185.
Mara, A., Schroeder, J., Chalouni, C. & Holley, S. A. 2007. Priming, initiation and synchronization of the segmentation clock by deltaD and deltaC. *Nat. Cell Biol.* **9**, 523–530.
Marchetti, M. C., Joanny, J. F., Ramaswamy, S., Liverpool, T. B., Prost, J., Rao, M. & Simha, R. A. 2013. Hydrodynamics of soft active matter. *Rev. Mod. Phys.* **85**, 1143–1189.
Marshall, W. F., Straight, A., Marko, J. F., Swedlow, J., Dernburg, A., Belmont, A., Murray, A. W., Agard, D. A. & Sedat, J. W. 1997. Interphase chromosomes undergo constrained diffusional motion in living cells. *Curr. Biol.* **7**, 930–939.
Masamizu, Y., Ohtsuka, T., Takashima, Y., Nagahara, H., Takenaka, Y., Yoshikawa, K., Okamura, H. & Kageyama, R. 2006. Real-time imaging of the somite segmentation clock: revelation of unstable oscillators in the individual presomitic mesoderm cells. *Proc. Natl Acad. Sci. USA* **103**, 1313–1318.
Morelli, L. G., Ares, S., Herrgen, L., Schroter, C., Julicher, F. & Oates, A. C. 2009. Delayed coupling theory of vertebrate segmentation. *HFSP J.* **3**, 55–66.
Morishita, Y., Kuroiwa, A. & Suzuki, T. 2015. Quantitative analysis of tissue deformation dynamics reveals three characteristic growth modes and globally aligned anisotropic tissue deformation during chick limb development. *Development* **142**, 1672–1683.
Nnetu, K. D., Knorr, M., Strehle, D., Zink, M. & Käs, J. A. 2012. Directed persistent motion maintains sheet integrity during multi-cellular spreading and migration. *Soft Matter* **8**, 6913.

Norden, C., Young, S., Link, B. A. & Harris, W. A. 2009. Actomyosin is the main driver of interkinetic nuclear migration in the retina. *Cell* **138**, 1195–1208.

Oates, A. C., Morelli, L. G. & Ares, S. 2012. Patterning embryos with oscillations: structure, function and dynamics of the vertebrate segmentation clock. *Development* **139**, 625–639.

Oginuma, M., Moncuquet, P., Xiong, F., Karoly, E., Chal, J., Guevorkian, K. & Pourquie, O. 2017. A gradient of glycolytic activity coordinates FGF and Wnt signaling during elongation of the body axis in amniote embryos. *Dev. Cell* **40**, 342–353. e310.

Ozbudak, E. M. & Lewis, J. 2008. Notch signalling synchronizes the zebrafish segmentation clock but is not needed to create somite boundaries. *PLoS Genet.* **4**, e15.

Peruani, F. & Morelli, L. G. 2007. Self-propelled particles with fluctuating speed and direction of motion in two dimensions. *Phys. Rev. Lett.* **99**, 010602.

Peruani, F., Deutsch, A. & Bar, M. 2006. Nonequilibrium clustering of self-propelled rods. *Phys. Rev. E Stat. Nonlin. Soft Matter Phys.* **74**, 030904.

Peruani, F., Nicola, E. M. & Morelli, L. G. 2010. Mobility induces global synchronization of oscillators in periodic extended systems. *New J. Phys.* **12**, 093029.

Pikovsky, A., Rosenblum, M. & Kurths, J. 2001. *Synchronization: A Universal Concept in Nonlinear Sciences*. Cambridge University Press, New York.

Pourquie, O. 2011. Vertebrate segmentation: from cyclic gene networks to scoliosis. *Cell* **145**, 650–663.

Qu, L., Long, F., Liu, X., Kim, S., Myers, E. & Peng, H. 2011. Simultaneous recognition and segmentation of cells: application in *C. elegans*. *Bioinformatics* **27**, 2895–2902.

Qu, L., Long, F. & Peng, H. 2015. 3-D Registration of Biological Images and Models: Registration of microscopic images and its uses in segmentation and annotation. *IEEE Signal Process. Mag.* **32**, 70–77.

Rafelski, S. M., Keller, L. C., Alberts, J. B. & Marshall, W. F. 2011. Apparent diffusive motion of centrin foci in living cells: implications for diffusion-based motion in centriole duplication. *Phys. Biol.* **8**, 026010.

Ramaswamy, S. 2010. The mechanics and statistics of active matter. *Annu. Rev. Condens. Matter Phys.* **1**, 323–345.

Riedel-Kruse, I. H., Muller, C. & Oates, A. C. 2007. Synchrony dynamics during initiation, failure, and rescue of the segmentation clock. *Science* **317**, 1911–1915.

Rieu, J. P., Upadhyaya, A., Glazier, J. A., Ouchi, N. B. & Sawada, Y. 2000. Diffusion and deformations of single hydra cells in cellular aggregates. *Biophys. J.* **79**, 1903–1914.

Rorth, P. 2009. Collective cell migration. *Annu. Rev. Cell Dev. Biol.* **25**, 407–429.

Saga, Y. 2012. The mechanism of somite formation in mice. *Curr. Opin. Genet. Dev.* **22**, 331–338.

Sawada, A., Shinya, M., Jiang, Y. J., Kawakami, A., Kuroiwa, A. & Takeda, H. 2001. Fgf/MAPK signalling is a crucial positional cue in somite boundary formation. *Development* **128**, 4873–4880.

Sbalzarini, I. F. & Koumoutsakos, P. 2005. Feature point tracking and trajectory analysis for video imaging in cell biology. *J. Struct. Biol.* **151**, 182–195.

Schroter, C., Ares, S., Morelli, L. G., Isakova, A., Hens, K., Soroldoni, D., Gajewski, M., Julicher, F., Maerkl, S. J., Deplancke, B. & Oates, A. C. 2012. Topology and dynamics of the zebrafish segmentation clock core circuit. *PLoS Biol.* **10**, e1001364.

Selmeczi, D., Mosler, S., Hagedorn, P. H., Larsen, N. B. & Flyvbjerg, H. 2005. Cell motility as persistent random motion: theories from experiments. *Biophys. J.* **89**, 912–931.

Sepulveda, N., Petitjean, L., Cochet, O., Grasland-Mongrain, E., Silberzan, P. & Hakim, V. 2013. Collective cell motion in an epithelial sheet can be quantitatively described by a stochastic interacting particle model. *PLoS Comput. Biol.* **9**, e1002944.

Shih, N. P., Francois, P., Delaune, E. A. & Amacher, S. L. 2015. Dynamics of the slowing segmentation clock reveal alternating two-segment periodicity. *Development* **142**, 1785–1793.

Shimojo, H., Isomura, A., Ohtsuka, T., Kori, H., Miyachi, H. & Kageyama, R. 2016. Oscillatory control of Delta-like1 in cell interactions regulates dynamic gene expression and tissue morphogenesis. *Genes Dev.* **30**, 102–116.

Skufca, J. D. & Bollt, E. M. 2004. Communication and synchronization in disconnected networks with dynamic topology: moving neighborhood networks. *Math. Biosci. Eng.* **1**, 1–13.

Soroldoni, D., Jorg, D. J., Morelli, L. G., Richmond, D. L., Schindelin, J., Julicher, F. & Oates, A. C. 2014. Genetic oscillations. A Doppler effect in embryonic pattern formation. *Science* **345**, 222–225.

Sprinzak, D., Lakhanpal, A., Lebon, L., Santat, L. A., Fontes, M. E., Anderson, G. A., Garcia-Ojalvo, J. & Elowitz, M. B. 2010. Cis-interactions between Notch and Delta generate mutually exclusive signalling states. *Nature* **465**, 86–90.

Stegmaier, J., Otte, J. C., Kobitski, A., *et al.* 2014. Fast segmentation of stained nuclei in terabyte-scale, time resolved 3D microscopy image stacks. *PLoS One* **9**, e90036.

Stegmaier, J., Amat, F., Lemon, W. C., McDole, K., Wan, Y., Teodoro, G., Mikut, R. & Keller, P. J. 2016. Real-time three-dimensional cell segmentation in large-scale microscopy data of developing embryos. *Dev. Cell* **36**, 225–240.

Steventon, B., Duarte, F., Lagadec, R., Mazan, S., Nicolas, J. F. & Hirsinger, E. 2016. Species-specific contribution of volumetric growth and tissue convergence to posterior body elongation in vertebrates. *Development* **143**, 1732–1741.

Szabo, B., Szollosi, G. J., Gonci, B., Juranyi, Z., Selmeczi, D. & Vicsek, T. 2006. Phase transition in the collective migration of tissue cells: experiment and model. *Phys. Rev. E* **74**, 061908.

Szabo, A., Unnep, R., Mehes, E., Twal, W. O., Argraves, W. S., Cao, Y. & Czirok, A. 2010. Collective cell motion in endothelial monolayers. *Phys. Biol.* **7**, 046007.

Takagi, H., Sato, M. J., Yanagida, T. & Ueda, M. 2008. Functional analysis of spontaneous cell movement under different physiological conditions. *PLoS One* **3**, e2648.

Tambe, D. T., Hardin, C. C., Angelini, T. E., Rajendran, K., Park, C. Y., Serra-Picamal, X., Zhou, E. H., Zaman, M. H., Butler, J. P., Weitz, D. A., Fredberg, J. J. & Trepat, X. 2011. Collective cell guidance by cooperative intercellular forces. *Nat. Mater.* **10**, 469–475.

Upadhyaya, A., Rieu, J. P., Glazier, J. A. & Sawada, Y. 2001. Anomalous diffusion and non-Gaussian velocity distribution of *Hydra* cells in cellular aggregates. *Phys. A* **293**, 549–558.

Uriu, K. 2016. Genetic oscillators in development. *Dev. Growth Differ.* **58**, 16–30.

Uriu, K. & Morelli, L. G. 2014. Collective cell movement promotes synchronization of coupled genetic oscillators. *Biophys. J.* **107**, 514–526.

Uriu, K., Morishita, Y. & Iwasa, Y. 2010. Random cell movement promotes synchronization of the segmentation clock. *Proc. Natl Acad. Sci. USA* **107**, 4979–4984.

Uriu, K., Ares, S., Oates, A. C. & Morelli, L. G. 2012. Optimal cellular mobility for synchronization arising from the gradual recovery of intercellular interactions. *Phys. Biol.* **9**, 036006.

Uriu, K., Ares, S., Oates, A. C. & Morelli, L. G. 2013. Dynamics of mobile coupled phase oscillators. *Phys. Rev. E* **87**, 032911.

Uriu, K., Morelli, L. G. & Oates, A. C. 2014. Interplay between intercellular signaling and cell movement in development. *Semin. Cell Dev. Biol.* **35**, 66–72.

Vedel, S., Tay, S., Johnston, D. M., Bruus, H. & Quake, S. R. 2013. Migration of cells in a social context. *Proc. Natl Acad. Sci. USA* **110**, 129–134.

Vedula, S. R., Leong, M. C., Lai, T. L., Hersen, P., Kabla, A. J., Lim, C. T. & Ladoux, B. 2012. Emerging modes of collective cell migration induced by geometrical constraints. *Proc. Natl Acad. Sci. USA* **109**, 12974–12979.

Vestergaard, C. L., Pedersen, J. N., Mortensen, K. I. & Flyvbjerg, H. 2015. Estimation of motility parameters from trajectory data. *Eur. Phys. J.* **224**, 1151–1168.

Vicsek, T. & Zafeiris, A. 2012. Collective motion. *Phys. Rep.* **517**, 71–140.

Vicsek, T., Czirok, A., Ben-Jacob, E., Cohen, I. I. & Shochet, O. 1995. Novel type of phase transition in a system of self-driven particles. *Phys. Rev. Lett.* **75**, 1226–1229.

Wang, P., Gonzalez, M. C., Hidalgo, C. A. & Barabasi, A. L. 2009. Understanding the spreading patterns of mobile phone viruses. *Science* **324**, 1071–1076.

Webb, A. B. & Oates, A. C. 2016. Timing by rhythms: daily clocks and developmental rulers. *Dev. Growth Differ.* **58**, 43–58.

Webb, A. B., Lengyel, I. M., Jorg, D. J., Valentin, G., Julicher, F., Morelli, L. G. & Oates, A. C. 2016. Persistence, period and precision of autonomous cellular oscillators from the zebrafish segmentation clock. *Elife* **5**, e08438.

Wright, G. J., Giudicelli, F., Soza-Ried, C., Hanisch, A., Ariza-Mcnaughton, L. & Lewis, J. 2011. DeltaC and DeltaD interact as Notch ligands in the zebrafish segmentation clock. *Development* **138**, 2947–2956.

Wu, P. H., Giri, A., Sun, S. X. & Wirtz, D. 2014. Three-dimensional cell migration does not follow a random walk. *Proc. Natl Acad. Sci. USA* **111**, 3949–3954.

Xiong, F., Tentner, A. R., Huang, P., Gelas, A., Mosaliganti, K. R., Souhait, L., Rannou, N., Swinburne, I. A., Obholzer, N. D., Cowgill, P. D., Schier, A. F.& Megason, S. G. 2013. Specified neural progenitors sort to form sharp domains after noisy Shh signaling. *Cell* **153**, 550–561.

Yabe, T. & Takada, S. 2016. Molecular mechanism for cyclic generation of somites: lessons from mice and zebrafish. *Dev. Growth Differ.* **58**, 31–42.

Yamaguchi, Y., Suzuki, T., Mizoro, Y., Kori, H., Okada, K., Chen, Y., Fustin, J. M., Yamazaki, F., Mizuguchi, N., Zhang, J., Dong, X., Tsujimoto, G., Okuno, Y., Doi, M. & Okamura, H. 2013. Mice genetically deficient in vasopressin V1a and V1b receptors are resistant to jet lag. *Science* **342**, 85–90.

Zhou, C. & Kurths, J. 2005. Noise-sustained and controlled synchronization of stirred excitable media by external forcing. *New J. Phys.* **7**, 18.